Low-Intensity Pulsed Ultrasound Improves the Functional Properties of Cardiac Mesoangioblasts

Aurora Bernal · Laura M Pérez · Beatriz De Lucas · Nuria San Martín · Anke Kadow-Romacker · Gustavo Plaza · Kay Raum · Beatriz G. Gálvez

Abstract Cell-based therapy is a promising approach for many diseases, including ischemic heart disease. Cardiac mesoangioblasts are committed vessel-associated progenitors that can restore to a significant, although partial, extent, heart structure and function in a murine model of myocardial infarction. Low-intensity pulsed ultrasound (LIPUS) is a non-invasive form of mechanical energy that can be delivered into biological tissues as acoustic pressure waves, and is widely used for clinical applications including bone fracture healing. We hypothesized that the positive effects of LIPUS on bone and soft tissue, such as increased cell differentiation and cytoskeleton reorganization, could be applied to increase the therapeutic potential of mesoangioblasts for heart repair. In this work, we show that LIPUS stimulation of cardiac mesoangioblasts isolated from mouse and human heart results in significant cellular modifications that provide beneficial effects to the cells, including increased malleability and improved motility. Additionally, LIPUS stimulation increased the number of binucleated cells and induced cardiac differentiation to an extent comparable with 5′-azacytidine treatment. Mechanistically, LIPUS stimulation activated the BMP-Smad signalling pathway and increased the expression of myosin light chain-2 together with upregulation of β1 integrin and RhoA, highlighting a potentially important role for cytoskeleton reorganization. Taken together, these results provide functional evidence that LIPUS might be a useful tool to explore in the field of heart cell therapy.

Keywords LIPUS · Cardiac mesoangioblasts · Migration · Differentiation · Cytoskeleton

Introduction

Acute myocardial infarction is a leading cause of death worldwide [1, 2]. Myocardial infarction results in cardiomyocyte apoptosis and necrosis, leading to an irreversible loss of myocardium and replacement with scar tissue [3]. Patients who survive the immediate event suffer a marked reduction in myocyte number and are prone to cardiac pump dysfunction [4].

Cardiac mesoangioblasts (CMAs) are vessel-associated mesenchymal stem cells derived from the heart that can differentiate efficiently into mature cardiomyocytes [5–7]. Previous results have shown that CMAs restore to a significant, although partial, heart structure and function in a murine coronary artery ligation model [5]. One of the principal reasons for the incomplete effectiveness of CMAs in this model is likely the inadequate homing of these cells to the heart [5]. CMA extravasation requires selective precursor-endothelial cell recognition [8], as leukocytes require it during homing inflammatory processes [9–11]. These interactions are

mediated by adhesion molecules and cytokines coordinated response [12]. Homing is determined by target tissue cytokines expression profile as well the repertoire of expressed receptors [13, 14]. Not only some adhesion molecules such as β2-integrin [15], but also cytokines are also are involved on cell extravasation. For instances, SDF-1 and VEGF favour the arrest of progenitors on the vascular endothelium, whereas IL-8 promotes stem cells mobilization from de bone marrow [16–18]. Besides HMGB-1 and TNF-α play a role as signals to induce cell migration [19–21]. Because of some of the key molecules that control rolling and extravasation of leukocytes, such as L-selectin or b2-integrin [22, 23] are not expressed by CMAs [24], further investigation about CMA-based therapy in post-MI treatment is required to increase its efficiency [5]. Accordingly, L-selectin expression and exposure of cells to Sdf-1 improves homing of CMAs to the infarcted free wall of the heart and aids recovery of left ventricular wall motion after infarction [24]. However, for CMAs to be used as efficient tools for post-MI treatment, some challenges still remain, especially with regards to achieving higher repair rates and limiting the manipulation of replacement cells [4].

Low-intensity pulsed ultrasound (LIPUS) is a non-invasive modality in which a mechanical stimulus is transmitted transcutaneously into biological tissues as high-frequency, small-amplitude and pulsed pressure waves [25]. LIPUS stimulation has been reported to accelerate bone maturation in animal models [26] and in clinical treatments [27], and is increasingly used as a non invasive therapy option to promote bone and wound healing [28, 29]. Indeed, LIPUS stimulation promotes a plethora of extra-, inter-, and intracellular events, which result in improved bone and soft tissue repair [30]. Among other reported effects, LIPUS stimulation promotes cell proliferation and DNA synthesis in skin fibroblasts [31], osteogenesis [32–34], protein synthesis [35, 36], and calcium uptake in osteoblasts, gingival fibroblasts, and periosteal cells [37], but not in chondrocytes [38, 39]. The effects of LIPUS on intercellular activity, cytokine release [40], gene expression [41], calcium mineralization [42], Akt signaling [43], potassium influx [44], angiogenesis [45, 46], adenyl cyclase activity and TGFβ synthesis [36] have all been studied previously. Further, LIPUS stimulation has been shown to induce the formation of actin stress fibres and focal adhesions in addition to cytoskeleton reorganization [31]. Taken together, these attributes indicate that LIPUS might be a beneficial modality for many types of tissue injury.

Although it has been reported LIPUS induces angiogenesis in a porcine model of chronic myocardiac ischemia [46], the potential repair of LIPUS for cardiovascular disease is already not known. We hypothesized that the stimulatory effects of LIPUS in skin and bone tissue, such as cell differentiation and cytoskeleton dynamics, could be utilized to modify cardiac precursors in a novel strategy for heart repair. Here we have applied a focused LIPUS stimulation set up to stimulate CMAs and we demonstrate that it provokes significant cellular modifications that impact on cell shape, differentiation and migration in vitro. We have also examined the underlying mechanism by which this mechanical stimulus might promote cellular modification.

Materials and Methods

Reagents

Dulbecco's modified Eagle's medium (DMEM) and fetal bovine serum were purchased from Sigma (St. Louis, MO, USA). Penicillin, streptomycin, L-glutamine and Hepes were from Lonza (Basel, Switzerland). The BdrU Incorporation Assay Kit was purchased from Merck Millipore (Billerica, MA, USA). The Violet Ratiometric Membrane Asymmetry Probe/Dead Cell Apoptosis Kit was purchased from Invitrogen (Carlsbad, CA, USA). The CytoSelect 48-well Cell Adhesion Assay was obtained from Cell Biolabs (San Diego, CA, USA). Transwell filters were from Corning Inc. (Acton, MA, USA). The Direct-zol RNA MiniPrep kit was purchased from (Zymo Research, Irvine CA, USA). Primary antibodies used were: monoclonal rabbit anti-myosin light chain 2, monoclonal rabbit anti-cardiac troponin, monoclonal mouse anti-cardiac troponin, monoclonal rabbit anti-sarcomeric actinin, polyclonal rabbit anti-occludin, polyclonal rabbit anti-β1-integrin, polyclonal rabbit anti-RhoA, polyclonal rabbit anti-β-actin, polyclonal rabbit anti-BMPR1A and monoclonal mouse anti-β1-integrin (all from Abcam, Cambridge, UK); polyclonal rabbit anti-α-actinin and polyclonal rabbit anti-phospho-Smad-1 (Ser463/465) / Smad-5 (Ser463/465) / Smad-8 (ser426-428) (Cell Signaling Technology, Danvers, MA, USA); polyclonal rabbit anti-connexin43 (Sigma); and monoclonal mouse anti-Bmp2 (R&D Systems, Minneapolis, MN, USA). Secondary antibodies used were: goat anti-rabbit HRP (Abcam); goat Alexa-488 anti-rabbit and goat Alexa-594 anti-mouse (Invitrogen) and goat anti-mouse HRP (Dako, Glostrup, Denmark). DAPI (4′, 6-diamino-2-phenylindole dihydrochloride) and ProLong Antifade reagent were from Invitrogen. Nitrocellulose membranes and the ECL system were purchased from GE Healthcare (Little Chalfont, UK). Unless otherwise stated, all other reagents were purchased from Sigma-Aldrich.

Isolation and Culture of Cardiac Mesoangioblasts

Cardiac mesoangioblasts (CMAs) were isolated from mouse and human ventricle explants, cloned and expanded as described [5, 8]. Mice were maintained and used in accordance with the National Institutes of Health Animal Care and Use Committee. Human CMAs were isolated from cardiac tissue obtained from male and female patients after cardiac surgery

procedures at the San Raffaele Hospital, Milano, Italy (age range from 56 to 76 years). Informed consent was obtained from all subjects and the sample collection conformed to the principles set out in the WMA Declaration of Helsinki and the NIH Belmont Report. Cells were cultured in complete Dulbecco's modified Eagles's medium (DMEM, Sigma, St. Louis MO, USA); containing 10 % FBS (Sigma, St. Louis MO, USA); penicillin/streptomycin (Pen/Strep) (Lonza, Basel, Switzerland); L-glutamine (Lonza); and Hepes (Lonza, Basel, Switzerland), at 37 °C in a humidified incubator at 5 % CO_2 /95 % air atmosphere. Cells at passage 10 were used for LIPUS stimulation. Cells at passage 5 post LIPUS stimulation were used for experiments as indicated. Cardiac differentiation of CMAs was induced in serum-free DMEM containing 10 μM 5′-azacytidine.

LIPUS Stimulation

CMAs (2.5×10^4) were seeded onto 24-multiwell plates in DMEM 10%FBS, Pen/Strp and HEPES, and placed inside the LIPUS stimulation chamber. From the 24 wells in the plate, 20 wells received consecutively a 5 MHz LIPUS stimulation in a custom-made Focused Low Intensity Pulsed Ultrasound device (Fig. 1) [47, 48]. For the stimulation, the well-plate was placed in an incubation chamber, which was mounted to a vertical translation stage. The ultrasound transducer (center frequency: 5 MHz, diameter: 15 mm, focal distance: 16.5 mm; beam width in focal plane: 0.48 mm; STT Richter, Muehlanger, Germany) was mounted to a two-axis horizontal translation stage and submersed in a temperature-controlled bath of sterilized, de-ionized, degassed water at 37 °C. The motion system allowed the precise positioning of incubation chamber and transducer with an accuracy of 1 μm. For the stimulation, the transducer was positioned centrally below a single well at a distance of 13.3 mm above the focus point of the transducer. The correct distance was controlled by measuring the time of flight of the signal reflected at the well-plate bottom. For the stimulation, the transducer was excited by an arbitrary waveform generator (33522A, Agilent, Keysight Technologies Santa Rosa, CA, USA) with a 5 MHz burst signal of 2 ms duration at a repetition rate of 100 Hz for 20 min. The output amplitude of 170 mV at the generator was amplified by a 25 W power amplifier (325LA, E&I, Rochester, NY, USA). Hardware components, positioning and stimulation was controlled by a PC using a custom toolbox developed MATLAB (Mathworks, Natick, MA, USA). The acoustic output power of 83 mW/cm^2 after propagation through the well-plate bottom was measured in continuous mode using an absorbing foam target connected to a balance [49]. The spatial average time average intensity for the burst stimulation I_{SATA}=16.2 mW/cm^2 was obtained by correcting the measured power value for focusing, burst mode excitation, and cross-sectional beam area at the well plate bottom with the correction factors K_{lens}=1.0867, K_{burst}=0.278, and a=0.8 cm^2, respectively. The -6 dB cross-sectional beam area of 0.8 cm^2 at the plate bottom (Fig. 1b) was measured using a lipstick hydrophone (Onda HGL-0400, Onda Corp. Sunnyvale, CA, USA). For this experiment, the transducers were excited with the same set-up as described above, except that only 10 cycles were used for the burst excitation. At the well edges, the intensity was approximately −12 dB lower compared to the maximum level in the center. No acoustic signals could be detected by the hydrophone in adjacent wells. The temperature in the well was measured by placing a thermocouple (LR316, JUMO GmbH & Co. KG, Fulda, Germany) directly above the well bottom, through a specially made aperture in the plate cover. No change of temperature by the ultrasound exposure could be observed.

The stimulation in the diverging far field of the transducer ensured direct coupling of the sound waves to the well-plate bottom through the water tank, and avoids both, temperature elevations in the well by transducer heating and the generation of standing waves between plate bottom and liquid air interface.

All cells were stimulated using the same protocol for 3 consecutive days. During this time, cells were in complete DMEM and maintained at 37 °C in a humidified 5 % CO_2 / 95 % air atmosphere. The 4 control wells did not receive LIPUS but were maintained under identical conditions. At 24 h post treatment, cells were collected and cryopreserved on FBS 10 % DMSO and maintained at −80 °C. For experimental procedures, cells were thawed in a 37 °C water bath, washed with DMEM by centrifugation and finally seed on DMEM 10 % FBS, Pen/Strp and HEPES. Each read-out was performed on more than five independent CMA samples.

LIPUS treatment dosage was determined according not only cell survival but also according F-actin cytoskeleton reorganization through F-actin staining as well as cell migration capacity through Transwell assay. To determine LIPUS dosage treatment cells were stimulated following the same protocol for 1 or 3 consecutive days, using the acoustic output power of 30 or 83 mW/cm^2. Finally, both F-actin staining and Transwell assay results pointed to the LIPUS dosage for 3 consecutive days using the acoustic output power of 83 mW/cm^2 as the most adequate to CMAs stimulation (Figure Sup. 1).

Cell Proliferation

Cell proliferation was quantified with the BdrU Incorporation Assay kit. Briefly, 5000 cells were seeded in 96-multiwell plates and BrdU was added to each well for 24 h. CMAs were then fixed and stained with an anti-BrdU antibody, followed by incubation with anti-mouse IgG HRP and peroxidase substrate. Incorporation of BrdU into the cell was measured with a Benchmark Plus microplate spectrophotometer (Bio Rad, Hercules CA, USA) at 450 nm and 540 nm.

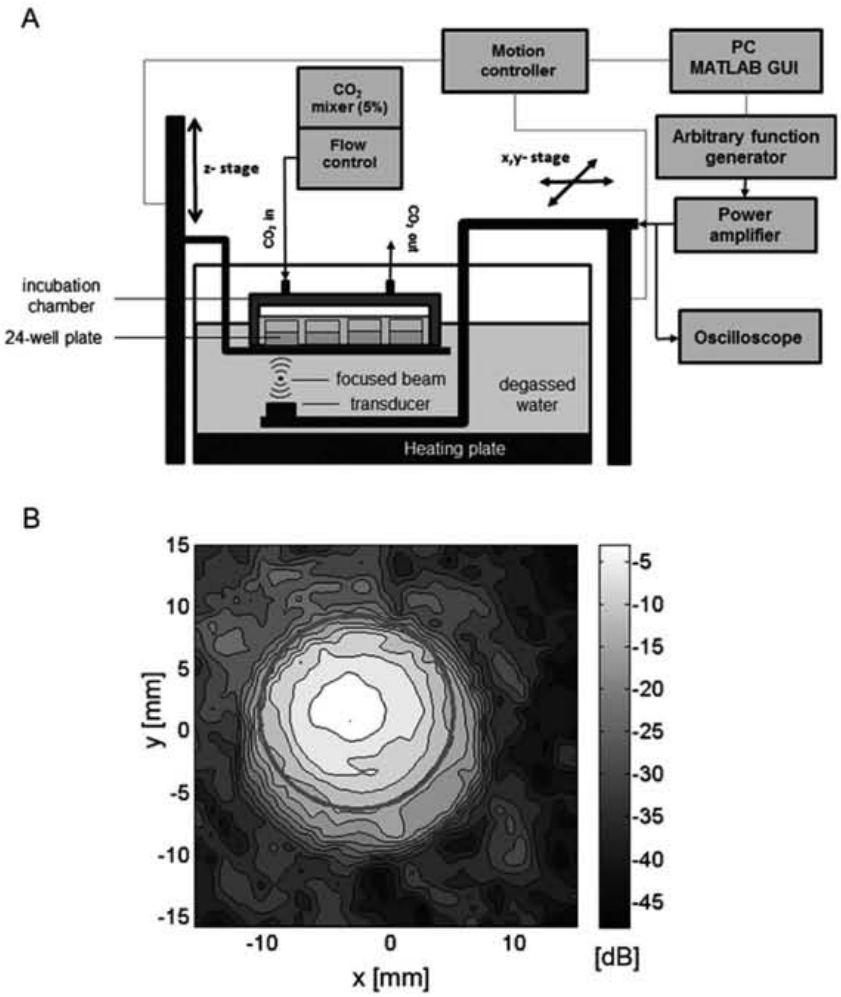

Fig. 1 Schematic setup of the focused stimulation system (**a**). A spherically focused 5-MHz transducer is positioned by an x,y scanning stage centrally below individual wells. The well plate is placed in an incubated chamber during the stimulation. The distance between transducer and the bottom of the well plate is adjusted by the z-scan stage and controlled by the measurement of the pulse-echo time of flight of the well-bottom reflection on the oscilloscope. Positioning and acoustic stimulation are controlled by a computer using a custom graphical user interface (GUI). The temporal peak intensity distribution measured by the hydrophone directly above the well-plate bottom is shown in (**b**)

Cell Viability Assessment

Apoptosis was measured using the Violet Ratiometric Membrane Asymmetry Probe/Dead Cell Apoptosis Kit [50], which also provides necrotic cells measures. Briefly, adhered cells were detached with trypsin and floating and adhered cells were collected and pelleted by centrifugation. Cells (10^6 cells/ml) were suspended in Hanks Balanced Salt Solution (HBSS) with 200nM 4′-N,N-diethylamino-6-(N,N,N-dodecyl-methylamino-sulfopropyl)-methyl-3-hydroxyflavone (F2N12S) and 1 mM SYTOX A Advanced dead cell stain solution, and incubated for 5 min at room temperature in the dark. Apoptosis measurements were performed with an LSRFortessa cytometer at 405 and 488 nm. Data were analyzed with BD FACSDiva Software.

Microcapillary Aspiration Assessment

Cell malleability was determined by measuring cell viscosity in a microcapillary aspiration test [51]. Cells were rinsed with trypsin-EDTA (0.05–0.02 %) for 2 min. After addition of serum-containing medium, cells were then centrifuged at 800 rpm for 5 min and suspended in growth medium. Micropipette aspiration experiments were performed using a custom-built device similar to that described previously [52] using microcapillaries with a nominal internal diameter of 10 μm. The cell suspension (~0.5 ml) was placed on a cover-glass plate and positioned in an optical Leica DMI3000B inverted microscope (Leica Microsystems, Wetzlar, Germany). The microcapillary was connected to a distilled water reservoir and differential pressure was applied by a difference in height of the reservoir with respect to the cell dispersion. This differential pressure ΔP was applied to facilitate the manipulations in two steps: the first one, 150 Pa, at the beginning of the experiment (t=0 s) and the second one, up to 400 Pa, after 20 s (t=20 s). The overall time of the experiment was 400 s. Cells were tested in the first three hours following treatment with trypsin at 25 °C. The aspiration process was studied by time-lapse imaging. Images were analyzed with ImageJ software (http://rsb.info.nih.gov/ij) to measure the length x of cellular material inside the

microcapillary. To quantify the volumes in the final situation, the volume inside the microcapillary was approximated by a cylinder and a hemisphere and the volume outside the microcapillary was approximated by an ellipsoid. The aspirated volume (V_{in}) was calculated as the volume inside the microcapillary (cylinder plus hemisphere) minus the spherical cap corresponding to the initial volume of the cell inside the microcapillary. Finally, the apparent viscosity of the cells was computed using the linearized equation obtained by Needham and Hochmuth [53].

Assessment of Cell Matrix Adhesion

Cell matrix adhesion capacity was determined with the CytoSelect 48-well Cell Adhesion Assay [54]. Briefly, 10^5 cells suspended in complete DMEM were added to individual wells of a 48-multiwell plate for 1 h and then medium was discarded. The remaining attached cells were stained and lysed with an extraction solution. Quantification of cell adhesion was performed on a Benchmark Plus microplate spectrophotometer at 560 nm.

Gene Expression Profiling

Total RNA was extracted from CMAs with Trizol Reagent (TriReagent) and concentration was quantified in a spectrophotometer (ND1000 NanoDrop, Thermofisher Scientific, Waltham, MA, USA). RNA integrity was monitored by ethidium bromide staining after agarose gel electrophoresis. RNA was reverse-transcribed to cDNA using the High Capacity cDNA Reverse Transcription Kit. PCR was performed using the Veriti 96w thermal cycler (Applied Biosystems Life Technologies, Paisley, UK) and PCR reaction mixtures contained cDNA templates, primers and 5Prime MasterMix (5Prime, Hamburg, Germany). Primers were designed using the Prime3 online program and checked with the Basic Local Alignment Search tool from NCBI. Thermal cycling parameters were 94 °C for 90 s; 35 cycles of 94 °C for 45 s, the primer-specific annealing temperature for 45 s and elongation at 72 °C for 60 s, and a final elongation at 72 °C for 10 min. PCR products were detected by ethidium bromide staining of 1.5 % agarose gels. PCR was performed using the following primers: β-actin (forward [Fw], CACGATGGAGG GGCCGGACTCAT; reverse [Rv], TAAAGA CCTCTATGCCAACACAG), GAPDH (Fw, AATGCA TCCTGCACCACCAA; Rv, GTGGCAGTGATGGCA TGGAC), Nkx2.5 (Fw, CAGTGGAGCTGGACAAAGCC; TAGCGACGGTTCTGGAACCA), Gata4 (Fw, CAGCATCTCTGTGGTCCTGA; Rv, GATGTTG TTGTGGCAAGTGG), c-actin (Fw, GTGCCAGG ATGTGTGACGA; Rv, CTGTCCCATACCCACCATGAC), Mef2c (Fw, AACACGGGGACTATGGGGATGGTA; Rv, TATGGCTGGACACTGGGATGGTA); connexin43 (Fw, GGACTGCTTCCTCTCACGTC; Rv, TTTGGAGATCCGC AGTCTTT) and cardiac troponin (Fw, CCACACGCCA AGAAAAAGTC; Rv, CGGCATAAGTCCTGAAGCTC).

Inmunofluorescence

Cells were plated on 0.1 % gelatin-coated coverslips, washed with PBS and fixed with 4 % paraformaldehyde for 10 min. Cells were treated with antigen retrieval buffer for 5 min at RT and blocked with 1 % donkey serum for 1 h. Antibody staining was carried out for 1 h at room temperature followed by detection with conjugated species-specific secondary antibodies for 1 h. Coverslips were co-stained with DAPI (300nM) for 30 min and mounted with ProLong Antifade reagent (Invitrogen) on glass slides. Images were obtained with a Leica DM2500/TCS SPE confocal microscope (Leica Microsystems). For filamentous actin (F-actin) staining, cells were incubated with phalloidin-TRITC (Sigma).

Quantification of Binucleated Cells

Cells were seeded in complete DMEM for 24 h and images of five randomly-selected 20× fields were recorded on an IX51 Inverted phase contrast microscope (Olympus America Inc., Center Valley, PA, USA), and binucleated cells were counted.

Wound Healing Assay

Confluent CMAs were scratch-wounded with a sterile micropipette tip. After removal of cellular debris, cells were allowed to migrate into the wounded area and photographs were taken each hour for 12 h with an IX51 inverted microscope (Olympus) using a 4× objective. Wound healing was determined by measuring the wound area using ImageJ software and values obtained were expressed as percentage of wound closure.

Cell Migration Assay

Cell migration was performed with Transwell chambers containing 8 μm pore size filters. Cells were plated at a density of 2×10^4 in 80 μl medium in the upper chamber of the Transwell and incubated for 24 h. After 24 h, filters were fixed with 4 % glutaraldehyde for 2 h and stained overnight with 2 % toluidine blue. Cells on the lower side of the filter were counted in five randomly-selected 10× fields using a bright-field microscope Nikon 90i (Nikon Instruments, Burgerweeshuispad, Amsterdam).

Cell Invasion Assay

The invasion assay was performed as per the migration assay, except that the membrane was coated beforehand with 1 % gelatin in PBS for 1 h at 37 °C.

Microarray

Total RNA was extracted as described from four independent LIPUS-stimulated CMA samples using Trizol Reagent and the Direct-zol RNA MiniPrep Kit. The integrity of purified total RNA was determined in a 2100 Bioanalyzer (Agilent Technologies). A one-color microarray-based gene expression analysis protocol (Agilent Technologies, Palo Alto, CA, USA) was used to amplify and label RNA. Briefly, 200 ng of total RNA was reverse transcribed using the T7 promoter primer and MMLV-RT. Then, cDNA was converted to aRNA using T7 RNA polymerase, which simultaneously amplified target material and incorporated cyanine 3-labeled CTP. Samples were hybridized to Mouse GE 4x44K v2 Microarrays (G2519F-026655, Agilent Technologies). Cy3-labelled aRNA (1.65 μg) was hybridized for 17 h at 65 °C in a hybridization oven (G2545A, Agilent) set to 10 rpm, in a final concentration of 1X GEx Hybridization Buffer HI-RPM, according to manufacturer's instructions (One-Color Microarray-Based Gene Expression Analysis, Agilent Technologies). Arrays were then washed and dried out using a centrifuge. Next, arrays were scanned at 5 μm resolution on an Agilent DNA Microarray Scanner (G2565BA, Agilent Technologies) using the default settings for 4x44k format one-color arrays. Images provided by the scanner were analyzed using Feature Extraction V10 software (Agilent Technologies). Raw data files from Feature Extraction were imported into GeneSpring® GX software version 12.5 (Agilent Technologies). Quantile normalization was performed and log2 transformed expression values were obtained for each probe. Probes were also flagged (Detected, Not Detected) using GeneSpring® default settings [55]. Microarray data were analyzed using Ingenuity Pathway Analysis software.

Western Blot Analysis

Cell lysates were extracted and lysed directly in Laemmli buffer on ice. Lysates were resolved using 10 % SDS-PAGE and proteins were transferred to nitrocellulose membranes. Membranes were blocked with 5 % nonfat milk for 1 h at room temperature and subsequently incubated overnight at 4 °C with 1:1000 dilution of primary antibodies, followed by detection with the appropriate secondary antibody. Blots were visualized with ECL reagent and relative intensity of the specific bands was quantified by densitometry using ImageJ software (http://rsb.info.nih.gov/ij).

Data Analysis

Statistical analysis was performed using the GraphPad Prism software package (GraphPad, San Diego, CA, USA). Comparison of groups was performed with two-way analysis of variance. Values were expressed as mean±SEM, and data was considered significantly different when $p<0.05$.

Results

LIPUS Stimulation Modifies the Structural Features of CMAs

CMAs derived from mouse and human were stimulated with LIPUS for 20 min each day for a total of 3 days; after which, cells were cryopreserved. Macroscopic analysis of LIPUS-treated (US-treated) cells showed that, in contrast to untreated control CMAs which displayed a normal mesenchymal cell-like morphology and grew as homogenous monolayers in culture, US-treated cells were polygonal in shape and grew as clusters (Fig. 2a). Examination of cytoskeleton organization by rhodamine-phalloidin staining of F-actin confirmed that US-treated cells exhibited cellular clustering and also F-actin fibre reorganization (Fig. 2b). Questioning whether these changes affected the structural properties of US-treated cells, we analyzed cell-malleability and cell-matrix adhesion capacity. To determine malleability, cell viscosity was measured using a microcapillary aspiration test [51]. Results showed that US-treated mouse CMAs exhibited significantly less viscosity than equivalent control cells (Fig. 2c), demonstrating that LIPUS stimulation increased cell malleability. A similar trend was observed for US-treated human cells, although this did not reach significance (Fig. 2c). To analyze adhesion capacity, CMAs were allowed to attach to different extracellular matrix (ECM) components for 1 h. Compared with equivalent control cells, US-treated mouse and human cells displayed significantly reduced attachment to fibronectin, collagens I and IV and fibrinogen substrates, whereas attachment to laminin and BSA were comparable between conditions (Fig. 2d).

LIPUS stimulation had no effect on CMA proliferation measured as BrdU incorporation (Fig. 3a); however, apoptosis was significantly decreased in US-treated cells (Fig. 3b). Indeed, both mouse and human US-treated cells presented a larger proportion of live cells and a decreased number of early and late apoptotic cells (Fig. 3b). In contrast, no significant differences were found in necrosis between control and US-treated CMAs. Collectively, these findings indicate that although LIPUS stimulation does not modulate proliferative capacity, it promotes a decrease in apoptosis together with changes in the structural features of CMAs that might impact cellular mechanics and motility.

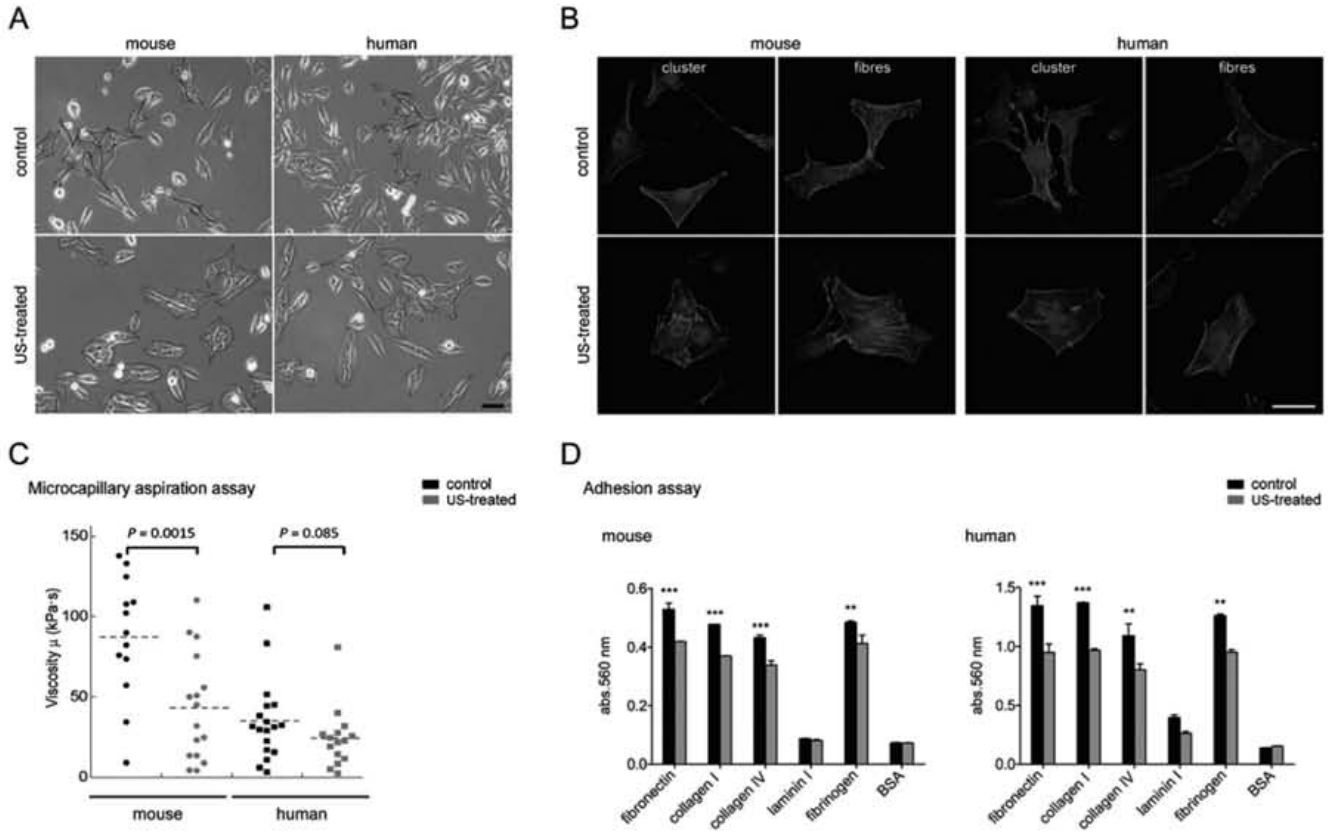

Fig. 2 LIPUS stimulation modifies the structural features of CMAs. **a** Cultured control and US-treated mouse and human CMAs were observed by phase contrast microscopy. Scale bar, 20 μm. **b** Confocal images of rhodamine-phalloidin stained F-actin (*red*) in control and US-treated mouse and human cells. Two representative images out of five independent experiments are shown illustrating cell clustering (cluster) and fibre reorganization (fibres). Nuclei were detected with DAPI (*blue*). Scale bar, 10 μm. **c** Cell malleability of control and US-treated mouse and human CMAs were determined by microcapillary aspiration assay. Data are from a representative experiment out of three independent experiments and denote the cellular viscosity, which is indirectly proportional to cell malleability. Discontinuous lines mark the mean data. **d** Cellular adhesion capacity of control and US-treated mouse and human CMAs was measured with a cell-matrix adhesion assay using fibronectin, collagen I, collagen IV, laminin I and fibrinogen; BSA was used as a no-matrix control. Data are from a representative experiment out of three independent experiments and denote mean±SEM absorbance (560 nm) from triplicate samples. ** $P<0.01$; *** $P<0.001$

LIPUS Stimulation Enhances CMA Motility and Invasion

Given the changes in structural organization and ECM engagement, we analyzed the motility and migratory capacity of CMAs using a scratch-wounding assay on confluent monolayers and followed the movement of cells into the injured area over 12 h. Interestingly, mouse and human US-treated CMAs demonstrated a significantly greater capacity to close the wound during the first 12 h for US-treated CMAs (Fig. 4a). Similar findings were observed in Transwell migration assays since the number of mouse and human CMAs located on the lower surface of the Transwell pore were significantly greater after LIPUS stimulation (Fig. 4b). To measure the invasion capacity of CMAs, Transwell pores were pre-coated with 1 % gelatin and cells were allowed to invade the lower chamber for 24 h. Consistent with the results from the migration assay, US-treated CMAs displayed a significantly greater capacity for invasion compared with equivalent control cells (Fig. 4c). Overall, these results demonstrate that LIPUS treatment significantly increases both cell migration and invasion capacity of CMAs.

LIPUS Stimulation of CMAs Induces Cardiac Differentiation

Cardiac mesoangioblasts are committed mesenchymal progenitors that express a panel of instructive cardiac transcription factors [56]. To evaluate whether LIPUS could modulate cardiac commitment, using immunocytochemistry we detected greater expression of structural cardiac proteins, including Conn43, TnT, sarcomeric α-actinin, α-actinin and occludin, in US-treated mouse and human CMAs relative to control cells (Fig. 5a). Consistent with our earlier observations, immunostaining also revealed differences in the morphology of US-treated cells. Moreover, closer inspection of growing US-treated CMAs revealed the presence of numerous binucleated cells in culture (Fig. 5b). Quantification of these cells established that 12 % of mouse and 8 % of human CMAs

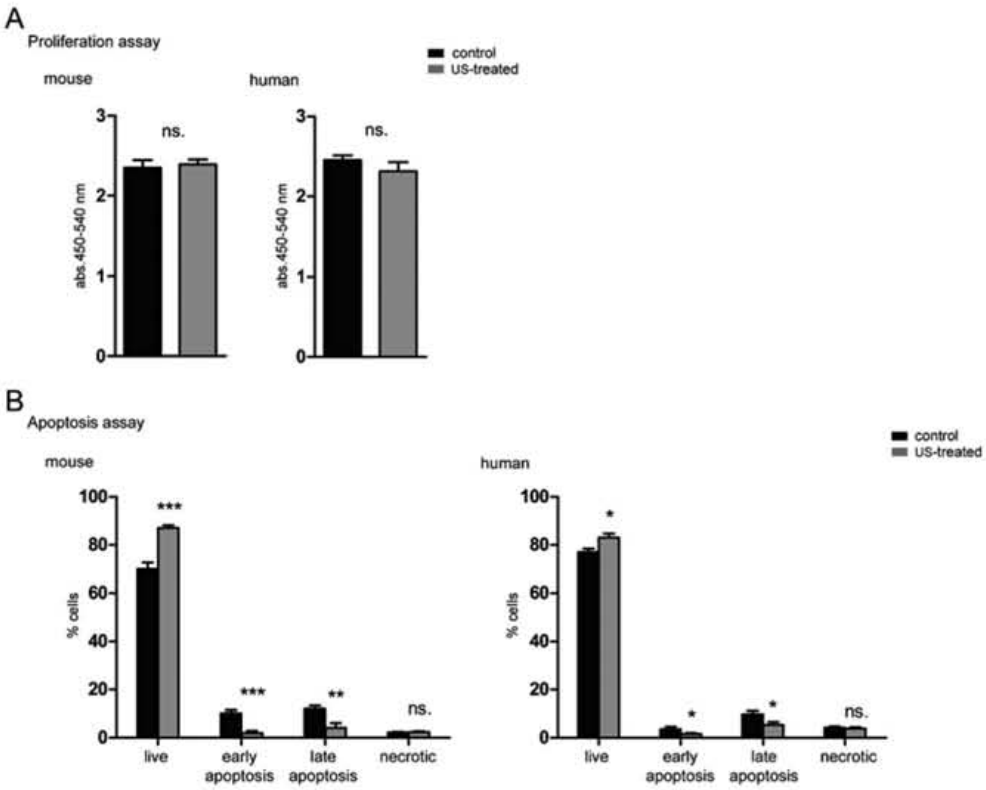

Fig. 3 Proliferation and viability of CMAs after LIPUS stimulation. **a** Proliferation was measured by BrdU incorporation in control and US-treated mouse and human CMAs. Data are from a representative experiment out of three independent experiments, performed in triplicate. **b** Cell death was measured in control and US-treated mouse and human CMAs using a ratiometric assay and quantified by flow cytometry. Data are from a representative experiment out of three independent experiments and denote mean±SEM from triplicate samples. NS, not significant; * $P<0.05$; ** $P<0.01$; *** $P<0.001$

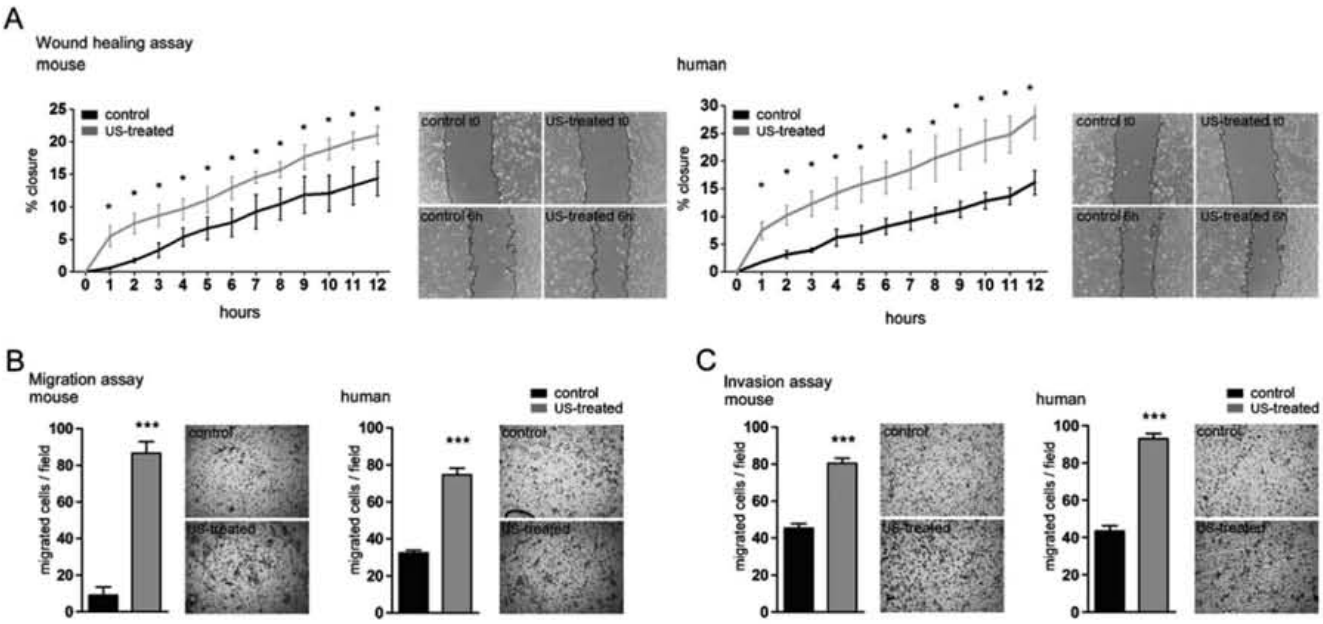

Fig. 4 LIPUS stimulation enhances CMA migration and invasion. **a** Wound-healing assay performed with control and US-treated mouse and human CMAs. Data are from a representative experiment out of three independent experiments performed and denote mean±SEM of wound closure percentage from triplicate samples at each hour over 24 h. A representative 4× image of the control and US-treated migrated cells after wound (t0) and 6 h later (6 h) are shown. Discontinuous lines mark the wound edge. **b** Transwell migration assay performed in control and US-treated mouse and human CMAs. Data are from a representative experiment out of three performed and denote mean±SEM of migrated cells/field of three independent experiments performed in triplicate. One representative image from five randomly selected 10× fields of control and US-treated migrated CMAs from mouse and human is shown. **c** Gel invasion assay using a gelatin-coated Transwell filter membrane was performed in control and US-treated mouse and human CMAs. Data represent the mean±SEM of migrated cells/field of three independent experiments performed in triplicate. One representative image from five randomly-selected 10× fields is shown. * $P<0.05$; ** $P<0.01$; *** $P<0.001$ compared versus CTRL-cells

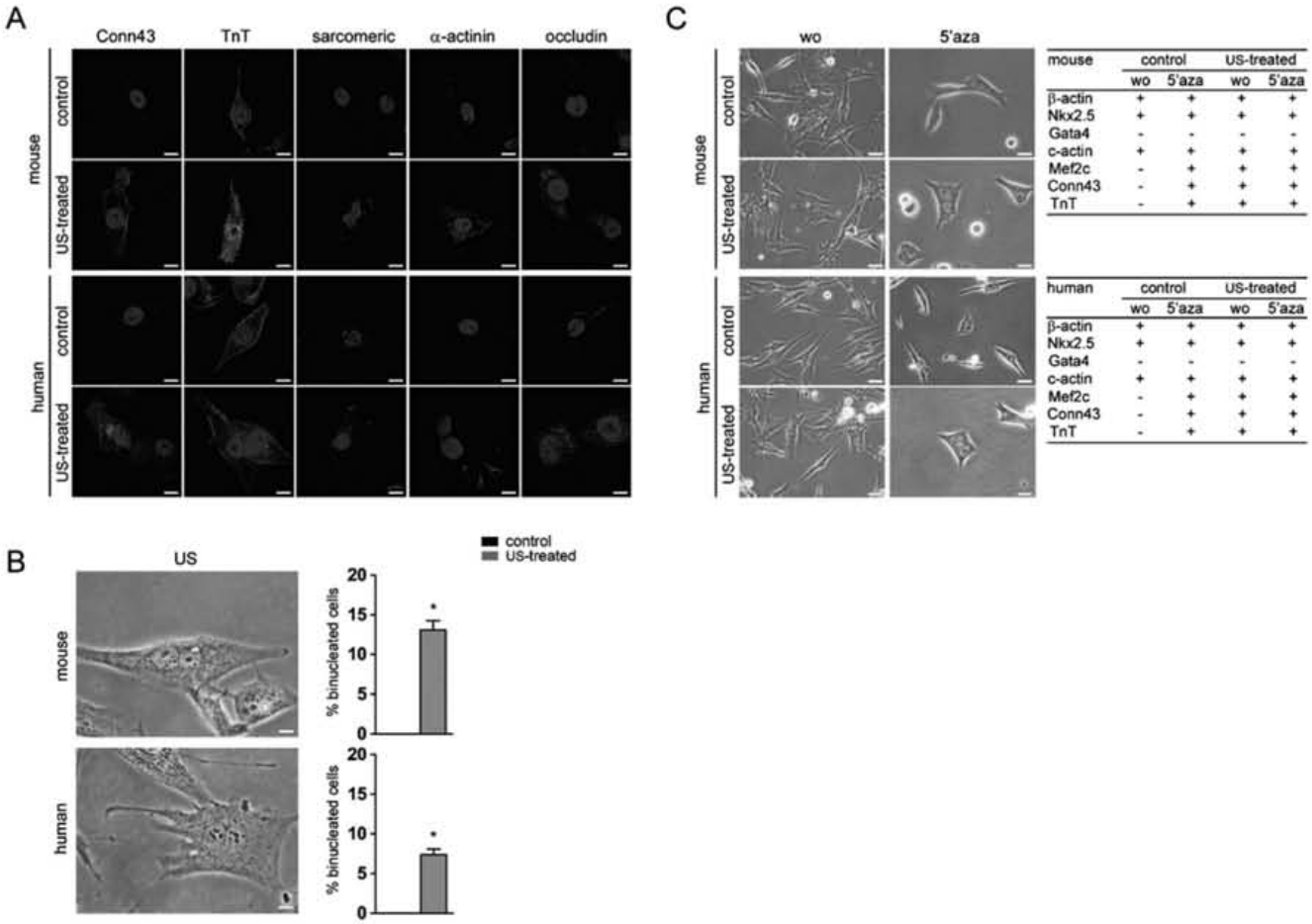

mouse	control		US-treated	
	wo	5'aza	wo	5'aza
β-actin	+	+	+	+
Nkx2.5	+	+	+	+
Gata4	-	-	-	-
c-actin	+	+	+	+
Mef2c	-	+	+	+
Conn43	-	+	+	+
TnT	-	+	+	+

human	control		US-treated	
	wo	5'aza	wo	5'aza
β-actin	+	+	+	+
Nkx2.5	+	+	+	+
Gata4	-	-	-	-
c-actin	+	+	+	+
Mef2c	-	+	+	+
Conn43	-	+	+	+
TnT	-	+	+	+

Fig. 5 LIPUS stimulation induces cardiac differentiation in CMAs. **a** Confocal microscopy of connexin43 (Conn43), troponin (TnT), sarcomeric α-actin, α-actinin and occludin (*green*) was performed by immunostaining of control and US-treated mouse and human CMAs. One representative image out of three independent experiments is shown. F-actin was detected with rhodamine-phalloidin (*red*) and nuclei were stained with DAPI (*blue*). Scale bar, 5 μm. **b** The presence of binucleated control and US-treated mouse and human CMAs in culture was observed by phase contrast microscopy. One representative image of five randomly-selected 40× fields is shown. Scale bar, 2.5 μm. Data represent the mean number of binuclear cells/field±SEM present in five randomly-selected 20× fields from three independent experiments performed in triplicate. * $P<0.05$. **c** Control and US-treated mouse and human CMAs were differentiated to the cardiac lineage with 10 μM 5′-azacytidine. One representative image out of three independent experiments performed in triplicate are shown, illustrating the change of cellular morphology and development of binucelate cells. Scale bar, 10 μm. Cardiac gene expression profiling was performed by PCR in control and US-treated mouse and human CMAs in the presence (5′-aza) or absence (wo) of 10 μM 5′-azacytidine: Nkx2.5, Gata4, c-actin, Mef2c, connexin43 (Conn43) and troponin (TnT), and also the housekeeping gene, β-actin. Results are summarized in the tables and describe expressed (+) and non-expressed (−) genes

were binucleated, whereas no binucleate cells were detected in control populations (Fig. 5b). Given the possibility that LIPUS stimulation may be triggering the emergence of cardiac progenitors, we compared this treatment with 5-azacytidine-induced cardiac differentiation. Similar to US-treated cells, results showed that mouse and human control CMAs exhibited morphology changes in the presence of 5′-azacytidine, becoming more polygonal in appearance with some binucleated cells developing (Fig. 5c). Gene expression profiling confirmed that LIPUS stimulation triggered cardiac commitment in CMAs and further showed that the effects were comparable with 5′-azacytidne treatment of control cells (Fig. 5c). Thus, LIPUS stimulation could emulate the effects of 5-azacytidine, suggesting that LIPUS stimulation enhances cardiac differentiation.

LIPUS stimulation increases expression of proteins involved in cardiomyocyte differentiation via BMP signalling and cytoskeleton reorganization through regulation of actin-based motility by Rho.

To explore the underlying mechanisms of LIPUS stimulation, a microarray analysis was performed on mouse CMAs treated or not to LIPUS. Results were confirmed by quantitative real time PCR (data not shown) and analyzed by Ingenuity Pathway Analysis (IPA) software. The most over-expressed gene in US-treated cells was myosin regulatory light chain 2, Myl2 (Figure Sup. 2a). Functional analysis with

IPA software identified cardiovascular system development and function, organ morphology and skeletal and muscular system development and function as the most significantly associated network with Myl2 (Figure Sup. 2b), and canonical pathway analysis revealed cardiomyocyte differentiation via Bone morphogenetic protein (BMP) receptors, chemokine signalling and regulation of actin-based motility by Rho as the most significant pathways in the input data set (Figure Sup. 2c). Reassuringly, western blotting confirmed the over-expression of Myl2 in US-treated mouse and human CMAs (Fig. 6a) and immunocytochemistry revealed significant Myl2 staining in US-treated but not control CMAs (Fig. 6a).

BMPs are involved in the regulation of many processes underlying cardiovascular development [57]. The BMP signalling pathway typically initiates with Bmp2 ligands binding BMP receptors leading to activation of p-Smad 1, 5 and 8, which then translocate to the nucleus and trigger cardiac differentiation [58]. Western blot analysis revealed a moderate increase in Bmp2 expression in US-treated CMAs (Fig. 6b) and p-Smad protein was similarly upregulated in US-treated CMAs compared with equivalent control cells (Fig. 6c).

Integrins are considered key players in the transduction of the ultrasound signal [59], and recent studies have shown an increase of β1-integrin expression in MSCs under mechanical stimulation [60]. Additionally, tension and stiffness are

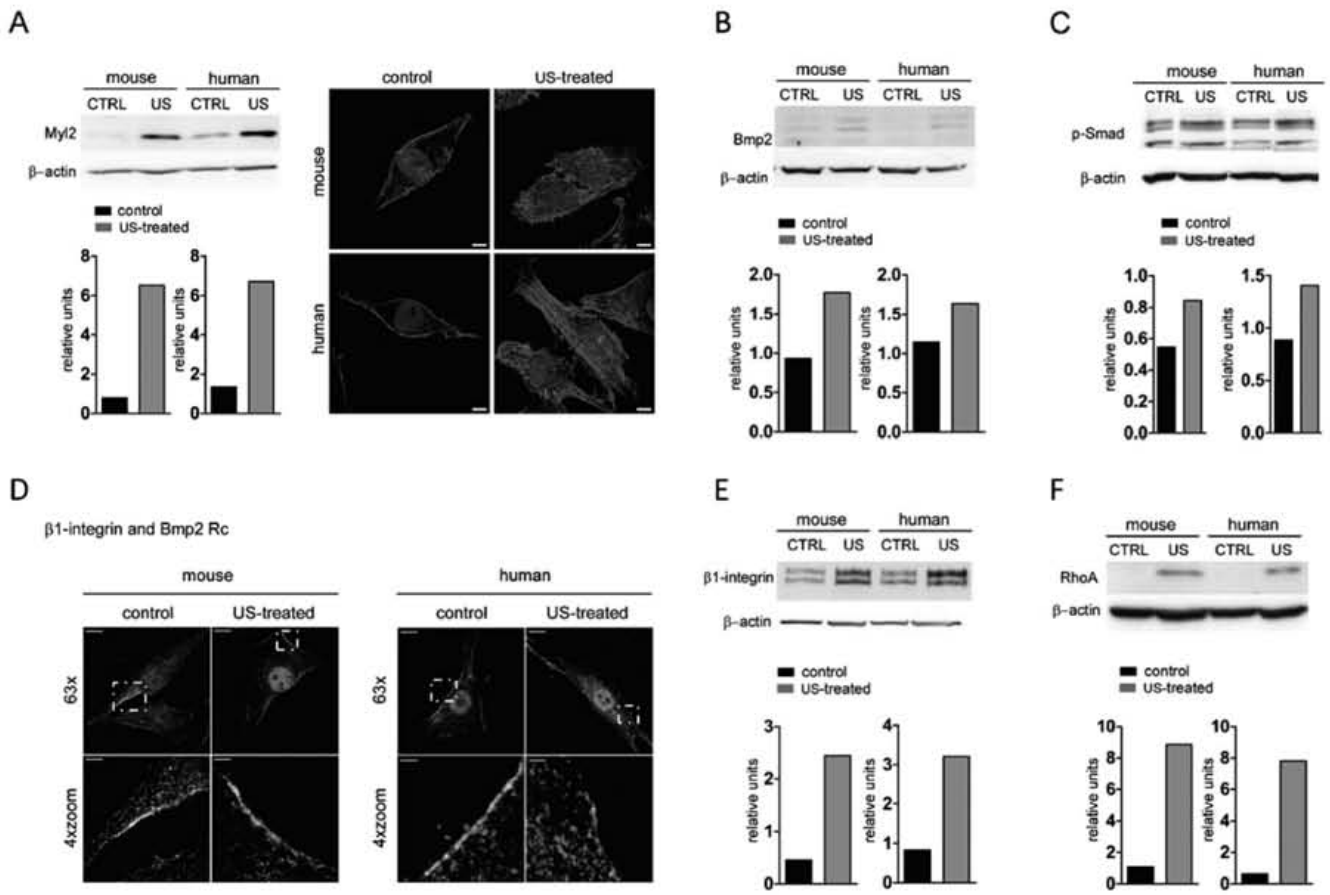

Fig. 6 LIPUS stimulation increases the expression of proteins involved in cardiomyocyte differentiation via BMP receptors, and augments cytoskeleton reorganization through regulation of actin-based motility by Rho. **a** Western blot and confocal images of Myl2 expression in control and US-treated mouse and human CMAs. Blot represents protein normalized to β-actin and is representative of three independent experiments. Graphic quantification of this representative blot is shown. Punctate Myl2 staining (*green*) can be observed in US-treated but not in control CMAs. F-actin was detected by rhodamine-phalloidin staining (*red*) and nuclei were stained with DAPI. Scale bar, 5 μm. One representative image out of three independent experiments is shown **b** Western blot analysis of Bmp2 expression in control and US-treated mouse and human CMAs. Blot represents protein normalized to β-actin and is representative of three independent experiments. Graphic quantification of this representative blot is shown. **c** Western blot analysis of pSmad expression in control and US-treated mouse and human CMAs. Blot represents protein normalized to β-actin and is representative of three independent experiments. Graphic quantification of this representative blot is shown. **d** Confocal microscopy of Bmp2 receptor (BMPR1A) (*green*) and β1-integrin (*red*) was performed by immunostaining of control and US-treated mouse and human CMAs. Nuclei were stained with DAPI. One representative image out of three independent experiments is shown. White discontinuous lines mark zoom areas. *Scale bar*, 10 μm; *zoom bar*, 2.5 μm. **e**, **f** Western blot analysis of β1-integrin and RhoA expression in control and US-treated mouse and human CMAs. Blots represent protein normalized to β-actin and are representative of three independent experiments. Graphic quantification of each representative blot is shown

sufficient for mechanical activation of β1-integrin [61], which also promotes the activation of BMP receptors, due to both of them colocalize [62]. We have confirmed both Bmp2 receptor and β1-integrin seem to colocalize on CMAs (Fig. 6d). Interestingly, mouse and human US-treated cells displayed significantly greater amounts of β1-integrin (Fig. 6e) Activated β1-integrin builds focal adhesions resulting in binding of F-actin, which acts as a bridge to link the integrin cytoplasmic domain to the cytoskeleton [63]. β1-integrin also activates integrin-associated signalling pathways, such as the Rho pathway [64], and it is known that mechanical stimulation may induce the formation of actin stress fibres and focal adhesions [65]. Since bioinformatics analysis predicted the regulation of actin-based motility by Rho as one of the most significant pathways of the input data set, and given that Rho/ROCK are involved in the reorganization of cytoskeletal components [66, 67], we also assessed RhoA expression by western blotting. Both mouse and human US-treated cells expressed a significantly greater amount of RhoA relative to equivalent control cells (Fig. 6f).

Overall, these results suggest that LIPUS stimulation induces an enhancement of cardiomyocyte differentiation, at least in part, via BMP receptors driving an increase in Bmp2 which, once outside of the cell, binds to the Bmp2 receptor to promote p-Smad 1, 5, 8 activation triggering cardiomyocyte differentiation. In addition, these results suggest that β1-integrin may acts as a mechanoreceptor to activate RhoA for F-actin cytoskeleton reorganization.

Discussion

In this study, we demonstrate that LIPUS stimulation has beneficial effects on cardiac mesoangioblasts and enhances cell motility and differentiation. These features are key factors for the successful use of this strategy as a new tool for the treatment of cardiac damage.

While apoptosis in CMAs was reduced by LIPUS stimulation, no changes were observed for proliferation, contrasting with findings in skin fibroblasts [31]; although in osteoblasts, LIPUS-stimulated proliferation is controversial [30] and may not be directly affected. Since LIPUS-induced mechanical stress has been shown to trigger mechanotransduction in cells [68], we examined several structural parameters in CMAs. LIPUS-treated cells grew in clusters and appeared more polygonal in shape with a reorganization of the F-actin cytoskeleton, which is consistent with observations in skin fibroblasts [31]. Further, LIPUS-treated cells were more malleable and less adhesive to ECM components. These changes correlated with a greater capacity for migration and invasion, indicating an increase in cell motility [69]. Although it has been reported

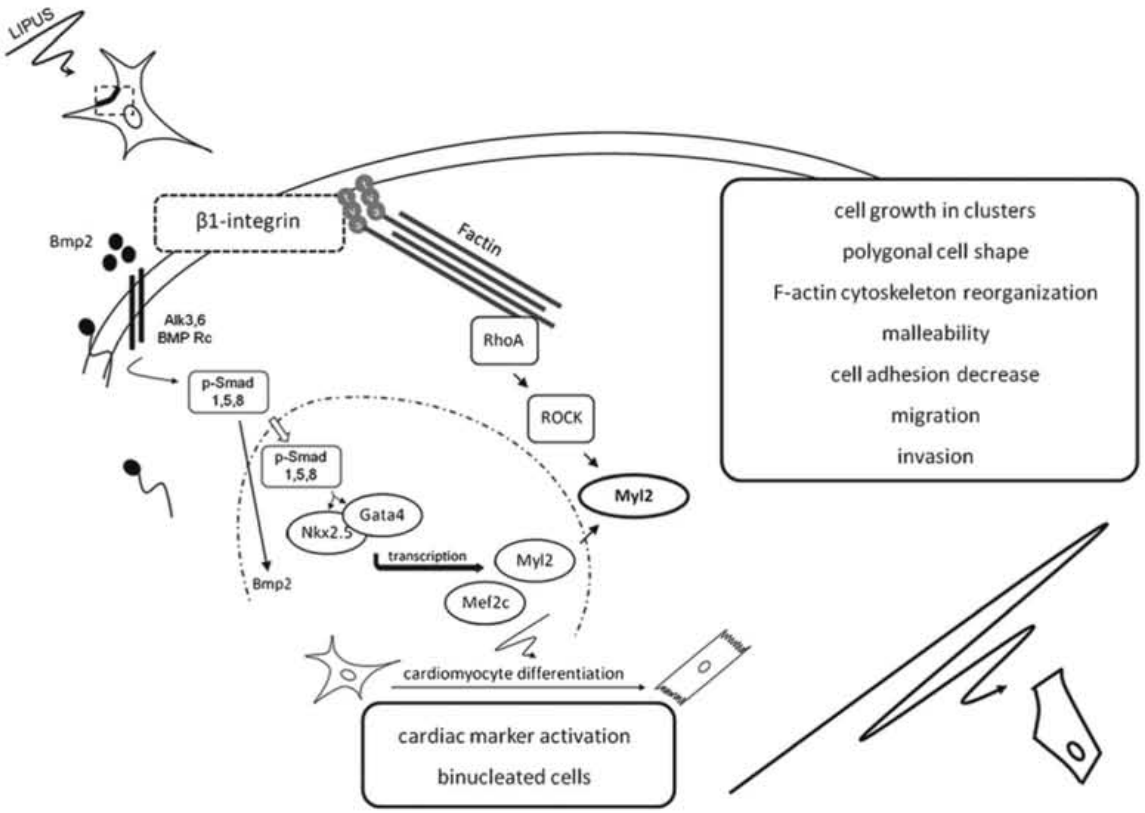

Fig. 7 LIPUS stimulation controls several factors which determine CMA cell fate. LIPUS appears to enhance cardiomyocyte differentiation via BMP receptors and cytoskeleton reorganization, through regulation of actin-based motility by Rho, improving CMA cell characteristics

LIPUS induces angiogenesis in a porcine model of chronic myocardiac ischemia [46], LIPUS have no effects in CMAs angiogenesis (data not shown). Interestingly, LIPUS treatment resulted in the appearance of binucleated cells, and cardiac differentiation was triggered as demonstrated by cardiac gene expression that was comparable to differentiation induced with 5′-azacytidine. These findings are reminiscent of the LIPUS-induced osteogenic differentiation of mesenchymal stem cells [35, 70].

Although the mechanism(s) of action of LIPUS remains to be elucidated in detail, our results suggest that β1-integrin might act as mechanoreceptor. Indeed, LIPUS fluid flow, created by either acoustic streaming or microstreaming, can modulate the extracellular matrix and apply shear stress, activating mechanoreceptors on the cell membranes [30]. Although other proteins, including ion channels and G-protein coupled receptors, have been proposed as candidate mechanoreceptors [71], it is known that integrins act as mechanotransducers in response to shear stress, mechanical stretch and cycled magnetic fields [72]. Specifically, integrins are thought of as key players in the transduction of the ultrasound signal [59] and recent studies have shown an increase of β1-integrin expression in MSCs under mechanical stimulation [60]. Additionally, tension and stiffness are sufficient for mechanical activation of β1-integrin [61].

Given this information, we propose (Fig. 7) that LIPUS arrives to the cell membrane and might trigger a conformational change in β1-integrin to the active form. This, in turn, might build focal adhesion and also promotes the activation of BMP receptors, activating p-Smad 1, 5 and 8. Increased Bmp-Smad signalling then activates cardiac transcription factors such as Nkx2.5, Mef2c and Myl2 [58]. This phenomenon establishes a positive feed-back since p-Smad 1, 5, 8 are also involved in Bmp2 transcription [73], which once transcribed, exits the cell by virtue of it signal peptide, and can bind its receptor. Indeed, a synergistic effect between mechanical loading and Bmp2 treatment has been reported [74, 75], in accordance with our results. Additionally, after LIPUS stimulation, β1-integrin becomes active and builds focal adhesions, linking finally to F-actin, which undergoes reorganization [76]. We have confirmed that US-treated cells have a higher quantity of RhoA, which targets ROCK. Subsequently, ROCK phosphorylates Myl2 resulting in activity, and also phosphorylates and inhibits Myl2-phosphatase, thus potentiating Myl2 activation [77].

In summary, LIPUS action on β1-integrin would activate two pathways: cardiomyocyte differentiation via the BMP receptor, and F-actin cytoskeleton reorganization mediated by RhoA; both these pathways converge on Myl2 activation. Cardiac differentiation via BMP receptor signalling results in cardiac marker activation and the appearance of binucleated cells resembling cardiomyocytes. Also, F-actin cytoskeleton reorganization mediated by RhoA would be the origin of structural changes related with the increase of malleability and the decrease of cell-matrix adhesion, both of which are related with cell motility enhancement.

In conclusion, LIPUS stimulation leads to beneficial effects on cardiac mesoangioblasts by enhancing advantageous cell features for their use after cardiac damage. Our results suggest LIPUS might be a potential tool to explore in the field of cardiac cell therapy.

Acknowledgments We thank Kenneth McCreath for critical reading of the manuscript and Klaus-Vitold Jenderka for conducting the calibration measurements. AB, LMP, BL, NSM, AKR and GP researched data. AB, LMP, KR and BGG contributed to discussion and reviewed manuscript. ABM and BGG wrote the manuscript and discussed data.

Conflict of interest The authors declare no potential conflicts of interest.

References

Kikuchi, K., & Poss, K. D. (2012). Cardiac regenerative capacity and mechanisms. *Annual Review of Cell and Developmental Biology, 28*, 719–741.

Oh, H., Bradfute, S. B., Gallardo, T. D., Nakamura, T., Gaussin, V., et al. (2003). Cardiac progenitor cells from adult myocardium: homing, differentiation, and fusion after infarction. *Proceedings of the National Academy of Sciences of the United States of America, 100*, 12313–12318.

Huang, C., Gu, H., Yu, Q., Manukyan, M. C., Poynter, J. A., et al. (2011). Sca-1+ cardiac stem cells mediate acute cardioprotection via paracrine factor SDF-1 following myocardial ischemia/reperfusion. *PLoS One, 6*, e29246.

Bernal, A., & Galvez, B. G. (2013). The potential of stem cells in the treatment of cardiovascular diseases. *Stem Cell Reviews, 9*, 814–832.

Galvez, B. G., Sampaolesi, M., Barbuti, A., Crespi, A., Covarello, D., et al. (2008). Cardiac mesoangioblasts are committed, self-renewable progenitors, associated with small vessels of juvenile mouse ventricle. *Cell Death and Differentiation, 15*, 1417–1428.

Galvez, B. G., Covarello, D., Tolorenzi, R., Brunelli, S., Dellavalle, A., et al. (2009). Human cardiac mesoangioblasts isolated from hypertrophic cardiomyopathies are greatly reduced in proliferation and differentiation potency. *Cardiovascular Research, 83*, 707–716.

Vanelli, A., Pennarossa, G., Maffei, S., Galvez, B. G., Cossu, G., et al. (2012). Isolation, characterization and differentiation potential of cardiac progenitor cells in adult pigs. *Stem Cell Reviews, 8*, 706–719.

Bernal, A., Fernandez, M., Perez, L. M., San Martin, N., & Galvez, B. G. (2012). Method for obtaining committed adult mesenchymal precursors from skin and lung tissue. *PLoS One, 7*, e53215.

Peled, A., Kollet, O., Ponomaryov, T., Petit, I., Franitza, S., et al. (2000). The chemokine SDF-1 activates the integrins LFA-1, VLA-4, and VLA-5 on immature human CD34(+) cells: role in transendothelial/stromal migration and engraftment of NOD/SCID mice. *Blood, 95*, 3289–3296.

Butcher, E. C., & Picker, L. J. (1996). Lymphocyte homing and homeostasis. *Science, 272*, 60–66.

Frenette, P. S., Subbarao, S., Mazo, I. B., von Andrian, U. H., & Wagner, D. D. (1998). Endothelial selectins and vascular cell adhesion molecule-1 promote hematopoietic progenitor homing to bone

marrow. *Proceedings of the National Academy of Sciences of the United States of America, 95*, 14423–14428.

Schweitzer, K. M., Drager, A. M., van der Valk, P., Thijsen, S. F., Zevenbergen, A., et al. (1996). Constitutive expression of E-selectin and vascular cell adhesion molecule-1 on endothelial cells of hematopoietic tissues. *American Journal of Pathology, 148*, 165–175.

Campbell, J. J., Hedrick, J., Zlotnik, A., Siani, M. A., Thompson, D. A., et al. (1998). Chemokines and the arrest of lymphocytes rolling under flow conditions. *Science, 279*, 381–384.

Wright, D. E., Bowman, E. P., Wagers, A. J., Butcher, E. C., & Weissman, I. L. (2002). Hematopoietic stem cells are uniquely selective in their migratory response to chemokines. *Journal of Experimental Medicine, 195*, 1145–1154.

Yong, K. L., Watts, M., Shaun Thomas, N., Sullivan, A., Ings, S., et al. (1998). Transmigration of CD34+ cells across specialized and nonspecialized endothelium requires prior activation by growth factors and is mediated by PECAM-1 (CD31). *Blood, 91*, 1196–1205.

Peled, A., Grabovsky, V., Habler, L., Sandbank, J., Arenzana-Seisdedos, F., et al. (1999). The chemokine SDF-1 stimulates integrin-mediated arrest of CD34(+) cells on vascular endothelium under shear flow. *Journal of Clinical Investigation, 104*, 1199–1211.

Laterveer, L., Lindley, I. J., Heemskerk, D. P., Camps, J. A., Pauwels, E. K., et al. (1996). Rapid mobilization of hematopoietic progenitor cells in rhesus monkeys by a single intravenous injection of interleukin-8. *Blood, 87*, 781–788.

Grunewald, M., Avraham, I., Dor, Y., Bachar-Lustig, E., Itin, A., et al. (2006). VEGF-induced adult neovascularization: recruitment, retention, and role of accessory cells. *Cell, 124*, 175–189.

Galvez, B. G., San Martin, N., & Rodriguez, C. (2009). TNF-alpha is required for the attraction of mesenchymal precursors to white adipose tissue in Ob/ob mice. *PLoS One, 4*, e4444.

Galvez, B. G., Sampaolesi, M., Brunelli, S., Covarello, D., Gavina, M., et al. (2006). Complete repair of dystrophic skeletal muscle by mesoangioblasts with enhanced migration ability. *Journal of Cell Biology, 174*, 231–243.

Galvez, B. G., Matias-Roman, S., Yanez-Mo, M., Vicente-Manzanares, M., Sanchez-Madrid, F., et al. (2004). Caveolae are a novel pathway for membrane-type 1 matrix metalloproteinase traffic in human endothelial cells. *Molecular Biology of the Cell, 15*, 678–687.

Butcher, E. C. (1991). Leukocyte-endothelial cell recognition: three (or more) steps to specificity and diversity. *Cell, 67*, 1033–1036.

Springer, T. A. (1994). Traffic signals for lymphocyte recirculation and leukocyte emigration: the multistep paradigm. *Cell, 76*, 301–314.

Bernal, A., San Martin, N., Fernandez, M., Covarello, D., Molla, F., et al. (2012). L-selectin and SDF-1 enhance the migration of mouse and human cardiac mesoangioblasts. *Cell Death and Differentiation, 19*, 345–355.

Qin, L., Fok, P., Lu, H., Shi, S., Leng, Y., et al. (2006). Low intensity pulsed ultrasound increases the matrix hardness of the healing tissues at bone-tendon insertion-a partial patellectomy model in rabbits. *Clinical Biomechanics (Bristol, Avon), 21*, 387–394.

Mayr, E., Laule, A., Suger, G., Ruter, A., & Claes, L. (2001). Radiographic results of callus distraction aided by pulsed low-intensity ultrasound. *Journal of Orthopaedic Trauma, 15*, 407–414.

El-Mowafi, H., & Mohsen, M. (2005). The effect of low-intensity pulsed ultrasound on callus maturation in tibial distraction osteogenesis. *International Orthopaedics, 29*, 121–124.

Romano, C. L., Romano, D., & Logoluso, N. (2009). Low-intensity pulsed ultrasound for the treatment of bone delayed union or nonunion: a review. *Ultrasound in Medicine & Biology, 35*, 529–536.

Rubin, C., Bolander, M., Ryaby, J. P., & Hadjiargyrou, M. (2001). The use of low-intensity ultrasound to accelerate the healing of fractures. *Journal of Bone and Joint Surgery (American), 83-A*, 259–270.

Padilla, F., Puts, R., Vico, L., & Raum, K. (2014). Stimulation of bone repair with ultrasound: a review of the possible mechanic effects. *Ultrasonics, 54*, 1125–1145.

Zhou, S., Schmelz, A., Seufferlein, T., Li, Y., Zhao, J., et al. (2004). Molecular mechanisms of low intensity pulsed ultrasound in human skin fibroblasts. *Journal of Biological Chemistry, 279*, 54463–54469.

Schortinghuis, J., Bronckers, A. L., Stegenga, B., Raghoebar, G. M., & de Bont, L. G. (2005). Ultrasound to stimulate early bone formation in a distraction gap: a double blind randomised clinical pilot trial in the edentulous mandible. *Archives of Oral Biology, 50*, 411–420.

Cook, S.D., Ryaby, J.P., McCabe, J., Frey, J.J., Heckman, J.D., et al. (1997). Acceleration of tibia and distal radius fracture healing in patients who smoke. *Clinical Orthopaedics and Related Research* 198–207.

Ikeda, K., Takayama, T., Suzuki, N., Shimada, K., Otsuka, K., et al. (2006). Effects of low-intensity pulsed ultrasound on the differentiation of C2C12 cells. *Life Sciences, 79*, 1936–1943.

Suzuki, A., Takayama, T., Suzuki, N., Sato, M., Fukuda, T., et al. (2009). Daily low-intensity pulsed ultrasound-mediated osteogenic differentiation in rat osteoblasts. *Acta Biochimica et Biophysica Sinica (Shanghai), 41*, 108–115.

Naruse, K., Miyauchi, A., Itoman, M., & Mikuni-Takagaki, Y. (2003). Distinct anabolic response of osteoblast to low-intensity pulsed ultrasound. *Journal of Bone and Mineral Research, 18*, 360–369.

Leung, K.S., Cheung, W.H., Zhang, C., Lee, K.M., Lo, H.K. (2004). Low intensity pulsed ultrasound stimulates osteogenic activity of human periosteal cells. *Clinical Orthopaedics and Related Research* 253–259.

Zhang, Z. J., Huckle, J., Francomano, C. A., & Spencer, R. G. (2003). The effects of pulsed low-intensity ultrasound on chondrocyte viability, proliferation, gene expression and matrix production. *Ultrasound in Medicine & Biology, 29*, 1645–1651.

Parvizi, J., Wu, C. C., Lewallen, D. G., Greenleaf, J. F., & Bolander, M. E. (1999). Low-intensity ultrasound stimulates proteoglycan synthesis in rat chondrocytes by increasing aggrecan gene expression. *Journal of Orthopaedic Research, 17*, 488–494.

Li, J. K., Chang, W. H., Lin, J. C., Ruaan, R. C., Liu, H. C., et al. (2003). Cytokine release from osteoblasts in response to ultrasound stimulation. *Biomaterials, 24*, 2379–2385.

Yang, K. H., Parvizi, J., Wang, S. J., Lewallen, D. G., Kinnick, R. R., et al. (1996). Exposure to low-intensity ultrasound increases aggrecan gene expression in a rat femur fracture model. *Journal of Orthopaedic Research, 14*, 802–809.

Nolte, P. A., Klein-Nulend, J., Albers, G. H., Marti, R. K., Semeins, C. M., et al. (2001). Low-intensity ultrasound stimulates endochondral ossification in vitro. *Journal of Orthopaedic Research, 19*, 301–307.

Takeuchi, R., Ryo, A., Komitsu, N., Mikuni-Takagaki, Y., Fukui, A., et al. (2008). Low-intensity pulsed ultrasound activates the phosphatidylinositol 3 kinase/Akt pathway and stimulates the growth of chondrocytes in three-dimensional cultures: a basic science study. *Arthritis Research and Therapy, 10*, R77.

Chapman, I. V., MacNally, N. A., & Tucker, S. (1980). Ultrasound-induced changes in rates of influx and efflux of potassium ions in rat thymocytes in vitro. *Ultrasound in Medicine & Biology, 6*, 47–58.

Kaneko, T., Kimata, H., Sugimoto, H., Inoue, S., Ito, S., et al. (2002). Power Doppler ultrasonography for the assessment of vascular invasion by pancreatic cancer. *Pancreatology, 2*, 61–68.

Hanawa, K., Ito, K., Aizawa, K., Shindo, T., Nishimiya, K., et al. (2014). Low-intensity pulsed ultrasound induces angiogenesis and

ameliorates left ventricular dysfunction in a porcine model of chronic myocardial ischemia. *PLoS One, 9*, e104863.

Puts, R., Ambrosi, T., Kadow-Romacker, A., Raum, K., Ruschke, K., et al. (2014). In-vitro stimulation of cells of the musculoskeletal system with focused Low-Intensity Pulsed Ultrasound (FLIPUS): analyses of cellular activities in response to the optimized acoustic dose Ultrasonics Symposium (IUS). *IEEE International, 2014*, 1630–1633.

Puts, R., Ruschke, K., Kadow-Romacker, A., Hwang, S., Jenderka, K., et al. (2015). Mechanosensitive response of murine C2C12 myoblast to focused low-intensity pulsed ultrasound (FLIPUS) Stimulation ESUCB (in press).

Lewin, P. A., Barrie-Smith, N., Ide, M., Hynynen, K., & Macdonald, M. (2003). Interlaboratory acoustic power measurement. *Journal of Ultrasound in Medicine, 22*, 207–213.

Shynkar, V. V., Klymchenko, A. S., Kunzelmann, C., Duportail, G., Muller, C. D., et al. (2007). Fluorescent biomembrane probe for ratiometric detection of apoptosis. *Journal of the American Chemical Society, 129*, 2187–2193.

Hochmuth, R. M. (2000). Micropipette aspiration of living cells. *Journal of Biomechanics, 33*, 15–22.

Trickey, W. R., Lee, G. M., & Guilak, F. (2000). Viscoelastic properties of chondrocytes from normal and osteoarthritic human cartilage. *Journal of Orthopaedic Research, 18*, 891–898.

Yeung, A., & Evans, E. (1989). Cortical shell-liquid core model for passive flow of liquid-like spherical cells into micropipets. *Biophysical Journal, 56*, 139–149.

Cervera, A. M., Apostolova, N., Crespo, F. L., Mata, M., & McCreath, K. J. (2008). Cells silenced for SDHB expression display characteristic features of the tumor phenotype. *Cancer Research, 68*, 4058–4067.

Pradervand, S., Weber, J., Thomas, J., Bueno, M., Wirapati, P., et al. (2009). Impact of normalization on miRNA microarray expression profiling. *RNA, 15*, 493–501.

Minasi, M. G., Riminucci, M., De Angelis, L., Borello, U., Berarducci, B., et al. (2002). The meso-angioblast: a multipotent, self-renewing cell that originates from the dorsal aorta and differentiates into most mesodermal tissues. *Development, 129*, 2773–2783.

Tzeng, W. F., & Chen, Y. H. (1988). Suppression of snake-venom cardiotoxin-induced cardiomyocyte degeneration by blockage of Ca2+ influx or inhibition of non-lysosomal proteinases. *Biochemical Journal, 256*, 89–95.

van Wijk, B., Moorman, A. F., & van den Hoff, M. J. (2007). Role of bone morphogenetic proteins in cardiac differentiation. *Cardiovascular Research, 74*, 244–255.

Pounder, N. M., & Harrison, A. J. (2008). Low intensity pulsed ultrasound for fracture healing: a review of the clinical evidence and the associated biological mechanism of action. *Ultrasonics, 48*, 330–338.

Watabe, H., Furuhama, T., Tani-Ishii, N., & Mikuni-Takagaki, Y. (2011). Mechanotransduction activates alpha(5)beta(1) integrin and PI3K/Akt signaling pathways in mandibular osteoblasts. *Experimental Cell Research, 317*, 2642–2649.

Friedland, J. C., Lee, M. H., & Boettiger, D. (2009). Mechanically activated integrin switch controls alpha5beta1 function. *Science, 323*, 642–644.

Lai, C. F., & Cheng, S. L. (2005). Alphavbeta integrins play an essential role in BMP-2 induction of osteoblast differentiation. *Journal of Bone and Mineral Research, 20*, 330–340.

Ziegler, W. H., Gingras, A. R., Critchley, D. R., & Emsley, J. (2008). Integrin connections to the cytoskeleton through talin and vinculin. *Biochemical Society Transactions, 36*, 235–239.

Riveline, D., Zamir, E., Balaban, N. Q., Schwarz, U. S., Ishizaki, T., et al. (2001). Focal contacts as mechanosensors: externally applied local mechanical force induces growth of focal contacts by an mDia1-dependent and ROCK-independent mechanism. *Journal of Cell Biology, 153*, 1175–1186.

Pavalko, F. M., Chen, N. X., Turner, C. H., Burr, D. B., Atkinson, S., et al. (1998). Fluid shear-induced mechanical signaling in MC3T3-E1 osteoblasts requires cytoskeleton-integrin interactions. *American Journal of Physiology, 275*, C1591–C1601.

Ridley, A. J., & Hall, A. (1992). The small GTP-binding protein rho regulates the assembly of focal adhesions and actin stress fibers in response to growth factors. *Cell, 70*, 389–399.

Hotchin, N. A., & Hall, A. (1995). The assembly of integrin adhesion complexes requires both extracellular matrix and intracellular rho/rac GTPases. *Journal of Cell Biology, 131*, 1857–1865.

Whitney, N. P., Lamb, A. C., Louw, T. M., & Subramanian, A. (2012). Integrin-mediated mechanotransduction pathway of low-intensity continuous ultrasound in human chondrocytes. *Ultrasound in Medicine & Biology, 38*, 1734–1743.

Horwitz, A. R., & Parsons, J. T. (1999). Cell migration–movin' on. *Science, 286*, 1102–1103.

Uddin, S. M., & Qin, Y. X. (2013). Enhancement of osteogenic differentiation and proliferation in human mesenchymal stem cells by a modified low intensity ultrasound stimulation under simulated microgravity. *PLoS One, 8*, e73914.

Hoffman, B. D., Grashoff, C., & Schwartz, M. A. (2011). Dynamic molecular processes mediate cellular mechanotransduction. *Nature, 475*, 316–323.

Weyts, F. A., Li, Y. S., van Leeuwen, J., Weinans, H., & Chien, S. (2002). ERK activation and alpha v beta 3 integrin signaling through Shc recruitment in response to mechanical stimulation in human osteoblasts. *Journal of Cellular Biochemistry, 87*, 85–92.

Sant'Anna, E. F., Leven, R. M., Virdi, A. S., & Sumner, D. R. (2005). Effect of low intensity pulsed ultrasound and BMP-2 on rat bone marrow stromal cell gene expression. *Journal of Orthopaedic Research, 23*, 646–652.

Kopf, J., Petersen, A., Duda, G. N., & Knaus, P. (2012). BMP2 and mechanical loading cooperatively regulate immediate early signalling events in the BMP pathway. *BMC Biology, 10*, 37.

Schwarz, C., Wulsten, D., Ellinghaus, A., Lienau, J., Willie, B. M., et al. (2013). Mechanical load modulates the stimulatory effect of BMP2 in a rat nonunion model. *Tissue Engineering Part A, 19*, 247–254.

Hu, K., Ji, L., Applegate, K. T., Danuser, G., & Waterman-Storer, C. M. (2007). Differential transmission of actin motion within focal adhesions. *Science, 315*, 111–115.

Wang, Y., Zheng, X. R., Riddick, N., Bryden, M., Baur, W., et al. (2009). ROCK isoform regulation of myosin phosphatase and contractility in vascular smooth muscle cells. *Circulation Research, 104*, 531–540.